Finite-difference time domain method for light scattering by small ice crystals in three-dimensional space

Ping Yang and K. N. Liou

Department of Meteorology/Center for Atmospheric and Remote Sounding Studies, University of Utah, Salt Lake City, Utah 84112

Received November 2, 1995; revised manuscript received May 10, 1996; accepted May 16, 1996

The finite-difference time domain (FDTD) method for the solution of light scattering by nonspherical particles has been developed for small ice crystals of hexagonal shapes including solid and hollow columns, plates, and bullet rosettes commonly occurring in cirrus clouds. To account for absorption, we have introduced the effective permittivity and conductivity to circumvent the required complex calculations in the direct discretization of the basic Maxwell equations. In the construction of the finite-difference scheme for the time-marching iteration for the near field the mean values of dielectric constants are defined and evaluated by the Maxwell–Garnett rule. In computing the scattered field in the radiation zone (far field) and the absorption cross section, we have applied a new algorithm involving the integration of the electric field over the volume inside the scatterer on the basis of electromagnetic principles. This algorithm removes the high-angular-resolution requirement in integrating the scattered energy for the computation of the scattering cross section. The applicability and the accuracy of the FDTD technique in three-dimensional space are validated by comparison with Mie scattering results for a number of size parameters and wavelengths. We demonstrate that neither the conventional geometric optics method nor the Mie theory can be used to approximate the scattering, absorption, and polarization features for hexagonal ice crystals with size parameters from approximately 5 to 20.

1. INTRODUCTION

The scattering of electromagnetic waves by passive objects can be solved analytically for only some special geometries such as spheres,[1] infinite circular cylinders,[2–4] and spheroids.[5,6] For these shapes the variable-separation method can be applied to solve the vector wave equation. However, it appears unlikely that this approach can be employed to produce the scattering and absorption characteristics of hexagonal ice particles because of the difficulty involved in imposing the electromagnetic boundary condition at the particle surface. In the past the geometric optics principles have been extensively used to determine the scattering of light by hexagonal ice crystals.[7–10] However, the geometric optics approximation is valid only when the particle size is much larger than the incident wavelength. It has been shown by the present authors[11] that the localization of geometric rays in the ray-tracing procedure can lead to significant errors in scattering calculations if the size parameters are smaller than approximately 20 and 15 for the computations of phase function and cross sections, respectively, in the two-dimensional (2-D) case. The errors cannot be circumvented for small size parameters even by the novel geometric optics/integral equation hybrid method developed by the present authors[11] in which the shortcomings in the conventional geometric optics approach are largely removed.

Moreover, it is well known that the Rayleigh theory[12] can be applied to the scattering by a nonspherical particle with the size parameter much smaller than 1. There is a significant gap between the Rayleigh theory and the geometric optics approximation for the region of size parameters known as the resonant region.[13] Although numerous promising approaches, including the method of moments,[14,15] the discrete-dipole approximation,[16–18] the digitized Green-function technique,[19] the integral equation technique,[20] the T-matrix or extended boundary-condition method,[21,22] and the multiple-scattering approach,[23] have been developed for the solution of light scattering by small nonspherical particles, they are usually applicable to size parameters less than approximately 15 in practice and/or to specific shapes with smooth and continuous surfaces as a result of numerical stability requirements.

Small hexagonal ice crystals of less than 10 μm exist in cirrus clouds. There is a practical necessity to study the scattering of light by small ice crystals of various shapes illuminated by solar and thermal infrared radiation. In this paper the finite-difference time domain (FDTD) method, pioneered by electrical engineers,[24–28] and developed for a 2-D scattering problem by the present authors,[11] has been extended to a general three-dimensional (3-D) configuration, with specific applications to hexagonal ice crystals of various shapes. The FDTD technique solves the Maxwell equations in the time domain by using the finite-difference analog and is flexible for applications to light scattering by irregular particles. In Section 2 we first briefly summarize the conceptual basis for the FDTD method. In order to incorporate effectively the absorption, we have developed an efficient algorithm for the computation of the near field

0740-3232/96/1002072-14$10.00

and the transformation of the near field to the far field in 3-D space. Numerical validations of the FDTD solutions against the Mie results for spheres are presented in Section 3, where representative sample calculations for the scattering by solid and hollow hexagonal columns, plates, and bullet rosettes are also illustrated and discussed. Finally, conclusions are given in Section 4.

2. FINITE-DIFFERENCE TIME DOMAIN METHOD IN THREE-DIMENSIONAL SPACE

A. Conceptual Basis for the Finite-Difference Time Domain Technique

The FDTD technique is a direct implementation of Maxwell's time-dependent curl equations to solve the temporal variation of electromagnetic waves within a finite space that contains an object of arbitrary geometry and composition. In practice, the space is discretized by a grid mesh, and the existence of the scattering particle is defined by properly assigning the electromagnetic constants including permittivity, permeability, and conductivity over the grid points. The Maxwell curl equations are subsequently discretized by using finite-difference approximations in both time and space. At the initial time a plane-wave source, which does not require the harmonic condition, is turned on. The wave excited by the source will then propagate toward the scattering particle and eventually interact with it. The propagation and the scattering of the electromagnetic field are simulated by using the finite-difference analog of the Maxwell equations in the manner of time-marching iterations. Information on the convergent scattered field can be obtained when a steady-state field is established at each grid point if a continuous sinusoidal source is used, or when the field decreases to a significantly small value if a pulse source is used.

As stated above, the FDTD technique is used to solve the near field in a finite space within which the particle is embedded. However, the actual scattering processes of electromagnetic waves by a particle are in an unbounded space. Thus one must truncate the unlimited spatial region by introducing artificial boundaries in the application of the FDTD technique. In order that the simulated field within the truncated region be the same as that in the unbounded case, the artificial boundary must have the condition known as the absorbing or transmitting boundary condition[28,29]; otherwise, the spurious reflection of the boundary would contaminate the near field within the truncated domain. The construction of an efficient absorbing boundary condition is an important aspect of the FDTD technique and is still an active research topic.[30] The accuracy of the simulated results will be greatly affected by the performance of the absorbing boundary condition.

The near field computed by the finite-difference analog of the Maxwell equations is in the time domain. In order to obtain the frequency response of the scattering particle, we must transform the field from the time domain to the frequency domain. As pointed out in our previous study,[11] one can input a Gaussian pulse as an initial excitation and apply the discrete Fourier transform technique to obtain the frequency spectrum of time-dependent signals. In order to avoid numerical aliasing and dispersion, one must correctly select the width of the pulse and properly consider the available frequency spectrum provided by the pulse.

The scattering phase matrix, the single-scattering albedo, and the extinction cross section are determined by the scattered far field. Therefore it is required to transform the frequency response of the scattering particle from the near field to the far field. To achieve this goal, the common approach in applying the FDTD method is to invoke a surface-integration technique[25] on the basis of an equivalence principle that involves the tangential components of the electric and magnetic fields on a surface enclosing the particle.

The preceding four areas for the implementation of the FDTD technique have been extended to the numerical computation in the 3-D case. In addition, we also include particle absorption in the formulation, which was not done in our previous study. When a scatterer is absorptive, a direct discretization of the basic Maxwell equations for the computation of the near field will require complex calculations because of the nonzero imaginary part of the permittivity (or the refractive index) of the particle. Moreover, the transformation of the near field to the far field by the use of a surface-integration equation suffers from a number of shortcomings when absorption is involved, as will be discussed in Subsection 2.C. In order to circumvent these disadvantages, we have developed an efficient algorithm for the computation of the near field and for the transformation of the near field in 3-D space with the inclusion of particle absorption.

B. Finite-Difference Equations for Computing the Near Field in Three-Dimensional Space

Because ice is nonferromagnetic, we shall take the permeability, μ, as 1 throughout this investigation. Thus the source-free Maxwell time-dependent curl equations can be expressed by

$$\nabla \times \mathbf{H}(\mathbf{r}, t) = \frac{\epsilon}{c} \frac{\partial \mathbf{E}(\mathbf{r}, t)}{\partial t}, \tag{1a}$$

$$\nabla \times \mathbf{E}(\mathbf{r}, t) = -\frac{1}{c} \frac{\partial \mathbf{H}(\mathbf{r}, t)}{\partial t}, \tag{1b}$$

where ϵ is the permittivity of the dielectric medium, usually a complex variable, and c is the speed of light in vacuum. We should select a harmonic time-dependent factor of $\exp(-i\omega t)$ for the electromagnetic wave in the frequency domain so as to have a positive imaginary part of the refractive index. Thus we have

$$\epsilon = \epsilon_r + i\epsilon_i, \tag{2a}$$

$$\epsilon_r = m_r^2 - m_i^2, \qquad \epsilon_i = 2m_r m_i, \tag{2b}$$

where $i = \sqrt{-1}$ and m_r and m_i are the real and imaginary parts of the refractive index, respectively. When the medium is absorptive, i.e., m_i is nonzero, the complex calculation is required for Eq. (1a). It is well known that a complex operation is two times more expensive than a real operation in terms of the computer CPU time and memory requirement. To circumvent the complex operation, it is desirable to have an equivalent expression for

Eq. (1a) in which the complex permittivity can be avoided. For this reason we introduce an effective real permittivity, ϵ', and conductivity, σ, and rewrite the first Maxwell curl equation in a source-dependent form as follows:

$$\nabla \times \mathbf{H}(\mathbf{r}, t) = \frac{\epsilon'}{c} \frac{\partial \mathbf{E}(\mathbf{r}, t)}{\partial t} + \frac{4\pi}{c} \mathbf{J}(\mathbf{r}, t), \quad (3a)$$

where the second term on the right-hand side of the equation comes from the contribution of the effective electric current, which is given by

$$\mathbf{J}(\mathbf{r}, t) = \sigma \mathbf{E}(\mathbf{r}, t). \quad (3b)$$

Transforming Eqs. (1a) and (3a) to the equivalent equations in the frequency domain yields

$$\nabla \times \mathbf{H}(\mathbf{r}) = -ik\epsilon \mathbf{E}(\mathbf{r}), \quad (4a)$$

$$\nabla \times \mathbf{H}(\mathbf{r}) = -ik(\epsilon' + i4\pi\sigma/kc)\mathbf{E}(\mathbf{r}), \quad (4b)$$

where $k = \omega/c$ is the wave number of the electromagnetic wave in free space. From a comparison of Eqs. (4a) and (4b) it is clear that the two equations are equivalent if the following conditions hold:

$$\epsilon_r = \epsilon', \quad (5a)$$

$$\epsilon_i = 4\pi\sigma/kc. \quad (5b)$$

Using Eqs. (3) and (5), one can write the equivalent counterpart of Eq. (1a) as

$$\nabla \times \mathbf{H}(\mathbf{r}, t) = \frac{\epsilon_r}{c} \left[\frac{\partial \mathbf{E}(\mathbf{r}, t)}{\partial t} + \tau \mathbf{E}(\mathbf{r}, t) \right], \quad (6a)$$

$$\tau = kc\epsilon_i/\epsilon_r. \quad (6b)$$

At this point we can use Eqs. (1b) and (6) to construct the finite-difference analog of the Maxwell curl equations, which involves only real calculations. First, we need to discretize the equation in time. To do this, we rewrite Eq. (6a) in the form

$$\frac{\partial[\exp(\tau t)\mathbf{E}(\mathbf{r}, t)]}{\partial t} = \exp(\tau t) \frac{c}{\epsilon_r} \nabla \times \mathbf{H}(\mathbf{r}, t). \quad (7)$$

Integrating Eq. (7) over the time interval of $[n\Delta t,(n + 1)\Delta t]$, we obtain

$$\exp[\tau (n + 1)\nabla t]\mathbf{E}^{n+1}(\mathbf{r}) - \exp(\tau n\Delta t)\mathbf{E}^n(\mathbf{r}) = \int_{n\Delta t}^{(n+1)\Delta t} \exp(\tau t) \frac{c}{\epsilon_r} \nabla \times \mathbf{H}(\mathbf{r}, t) dt \approx \Delta t \exp[\tau (n + 1/2)\Delta t] \frac{c}{\epsilon_r} \nabla \times \mathbf{H}^{n+1/2}(\mathbf{r}). \quad (8)$$

It follows that

$$\mathbf{E}^{n+1}(\mathbf{r}) = \exp(-\tau\Delta t)\mathbf{E}^n(\mathbf{r}) + \exp(-\tau\Delta/2) \times \frac{c\Delta t}{\epsilon_r} \nabla \times \mathbf{H}^{n+1/2}(\mathbf{r}). \quad (9)$$

Similarly, for the magnetic field we have

$$\mathbf{H}^{n+1/2}(\mathbf{r}) = \mathbf{H}^{n-1/2}(\mathbf{r}) - C\Delta t \nabla \times \mathbf{E}^n(\mathbf{r}). \quad (10)$$

In the above equations the superscript n denotes that the associated field is evaluated at the time step $t = n\Delta t$.

As stated in Subsection 2.A, the space containing the scattering particle must be discretized by a number of grid cells. We use cubic cells in the 3-D case and evaluate the components of electric and magnetic fields on a cell at the staggered locations suggested by Yee,[24] as shown in Fig. 1. The advantage of such staggered positions is that the electromagnetic boundary conditions are guaranteed at the interfaces of the cells, so that the tangential components of the E field and the normal components of the H field are continuous at the interfaces. Next, we note that for an arbitrary vector, $\mathbf{f}$, the following relationship holds:

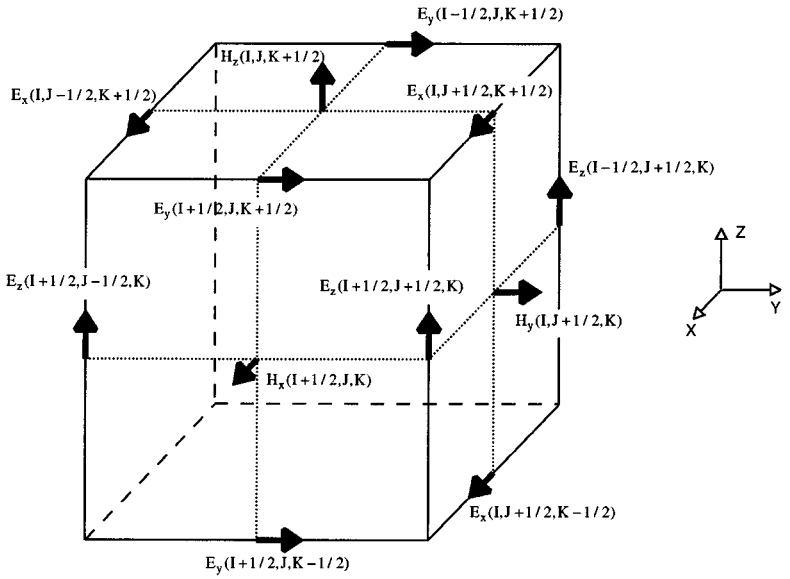

Fig. 1. Locations of the electric- and magnetic-field components on a cubic cell used in the numerical calculations.

$$\int\int \hat{n} \cdot (\nabla \times \mathbf{f})\mathrm{d}s = \oint \mathbf{f} \cdot \mathrm{d}^2\mathbf{l} \quad \text{(Stokes' theorem)}, \tag{11}$$

where $\hat{n}$ is the unit vector normal to the surface on which the integration is carried out and $\mathbf{l}$ is along the circumference of the surface. Applying Eq. (10) along with Eq. (11) to the top of the cell shown in Fig. 1, we obtain the following equation:

$$\int \int_{\text{top}} \hat{n} \cdot \mathbf{H}^{n\pm1/2}(\mathbf{r})\mathrm{d}^2s \approx (\Delta s)^2 H_z^{n\pm1/2}(I, J, K + 1/2), \tag{12a}$$

where Δs is the size of the cubic cell. We also have

$$\begin{aligned}\int \int_{\text{top}} \hat{n} \cdot [\nabla \times \mathbf{E}^n(\mathbf{r})]\mathrm{d}^2s &= \oint_{\text{top}} \mathbf{E}^n(\mathbf{r}) \cdot \mathrm{d}\mathbf{l} \\ &\approx \Delta s[E_y^n(I + 1/2, J, K + 1/2) \\ &\quad - E_y^n(I - 1/2, J, K) \\ &\quad + E_x^n(I, J - 1/2, K + 1/2) \\ &\quad - E_x^n(I, J + 1/2, K + 1/2)],\end{aligned} \tag{12b}$$

where $(I + 1/2, J, K + 1/2)$ denotes that the field component is evaluated at the location of $(x, y, z) = (I + 1/2, J, K + 1/2)\Delta s$. Applying the above procedure to Eqs. (9) and (10) for various field components, we can obtain the finite-difference analog of the Maxwell time-dependent equations. For example, the x components of the E and H fields can be computed by

$$\begin{aligned}E_x^{n+1}(I, J + 1/2, K + 1/2) &= \exp[-\Delta t\bar{\tau}(I, J + 1/2, K + 1/2)]E_x^n(I, J + 1/2, K + 1/2) + \exp[-\Delta t\bar{\tau}(I, J + 1/2, K + 1/2)/2] \frac{c\Delta t}{\Delta s\bar{\epsilon}_r(I, J + 1/2, K + 1/2)} [H_z^{n+1/2}(I, J + 1, K + 1/2) - H_z^{n+1/2}(I, J, K + 1/2) \\ &\quad + H_y^{n+1/2}(I, J + 1/2, K) \\ &\quad - H_y^{n+1/2}(I, J + 1/2, K + 1)],\end{aligned} \tag{13a}$$

$$\begin{aligned}H_x^{n+1/2}(I + 1/2, J, K) &= H_x^{n-1/2}(I + 1/2, J, K) + \frac{c\Delta t}{\Delta s} [E_z^n(I + 1/2, J - 1/2, K) - E_z^n(I + 1/2, J + 1/2, K) \\ &\quad + E_y^n(I + 1/2, J, K + 1/2) - E_y^n(I + 1/2, J, K - 1/2)],\end{aligned} \tag{13b}$$

where $\bar{\tau} = kc\bar{\epsilon}_i/\bar{\epsilon}_r$, in which $\bar{\epsilon}_r$ and $\bar{\epsilon}_i$ are the mean values of the real and the imaginary parts of the permittivity evaluated at the grid points, respectively. The Maxwell–Garnett rule is used to compute the mean permittivity in this study in an attempt to decrease the errors produced by the staircasing approximation.[11] Because ice is an optically thin medium in the visible and infrared wavelengths, the refractive index effect or the staircasing approximation for the scatterer is insignificant after the Maxwell–Garnett rule is applied to evaluate the mean dielectric constant over each grid size. Although the construction of Eqs. (13) is based on approximating the continuous integration by a quadrature formula, the derivation of these equations can also be made by applying the leapfrog difference quotients to discretize temporal and spatial derivatives in Eqs. (1b) and (6a). However, in the present approach the natural introduction of the mean permittivity will somehow offset the error produced by the staircasing approximation. It can be proven that the truncation error of the finite-difference analog of the Maxwell curl equations is of the second order in both time and space. Other schemes with truncation errors of high orders have been suggested,[31] but they are less practical. It is noted from Eqs. (13) that the E and H fields are interlaced in both time and space. The equations are in explicit forms in the time iteration; that is, once we input the initial electromagnetic field values, the propagation of the wave can be simulated by updating the E and H fields in a straightforward manner. For this reason the time-marching iteration in the computation of the near field by the FDTD technique is convenient and efficient. The electromagnetic field involved in Eqs. (13) is the total (incident + scattered) field. However, application of the absorbing boundary condition at the artificial boundary is required only to the outgoing induced or scattered field produced by the existence of the scattering particle. Following Mur[28] and Umashankar and Taflove,[25] we introduce an inner surface in the computational domain in which inside and on the inner surface the total field is evaluated, while, outside the surface, only the scattered field is computed. Since the fields computed in these two regions are not continuous, a connecting condition must be imposed at the inner surface. Suppose that the cells enclosed by the inner surface are those with indices of $I \in [IA, IB]$, $J \in [JA, JB]$, and $K \in [KA, KB]$. From Eqs. (13) the connecting condition at the surface can be obtained. For example, the x component of the E field is as follows:

$$\begin{aligned}\tilde{E}_x^{n+1}(I, JA - 1/2, K + 1/2) &= E_x^{n+1}(I, JA - 1/2, K + 1/2) - \frac{c\Delta t}{\Delta s} H_{o,z}^{n+1/2}(I, JA - 1, K + 1/2), \\ \tilde{E}_x^{n+1}(I, JB + 1/2, K + 1/2) &= E_x^{n+1}(I, JB + 1/2, K + 1/2) + \frac{c\Delta t}{\Delta s} H_{o,z}^{n+1/2}(I, JB + 1, K + 1/2), \\ &\quad K \in [KA - 1, KB],\end{aligned} \tag{14a}$$

$$\tilde{E}_x^{n+1}(I, J + 1/2, KA - 1/2) = E_x^{n+1}(I, J + 1/2, KA - 1/2) + \frac{c\Delta t}{\Delta s} H_{o,y}^{n+1/2}(I, J + 1, KA - 1),$$

$$\tilde{E}_x^{n+1}(I, J + 1/2, KB + 1/2) = E_x^{n+1}(I, J + 1/2, KB + 1/2) - \frac{c\Delta t}{\Delta s} H_{o,y}^{n+1/2}(I, J + 1/2, KB + 1),$$

$$J \in [JA - 1, JB], \tag{14b}$$

where $I \in [IA, IB]$, and the second terms with subscript o on the right-hand side of the above equations are the incident field and the first terms are those evaluated by the finite-difference equations given by Eqs. (13). In this way the governing equations are the same for both the scattered-field region and the total-field region except that the connecting conditions are imposed at the inner surface. The above connecting conditions, in principle, are the application of Schelkunoff's electromagnetic equivalence theorem.[32] As pointed out by Merewether *et al.*,[33] for the region inside the inner surface, the existence of the incident field can be defined by specifying the equivalent electric and magnetic currents on the surface. However, it is more straightforward to construct connecting conditions directly from the finite-difference equation given by Eqs. (13). In our previous study a global scattered-field formulation is constructed throughout the computational domain. It should be noted that the total-field algorithm presented in this paper is more accurate than the scattered-field algorithm, especially for the case involving a heavily shielded cavity or a metal object. In addition, the former is also more efficient because the specification of the incident wave is required only at the connecting surface. This is particularly significant in 3-D cases, since the CPU time is an important consideration in numerical simulations. Finally, for simplicity, we have used the same grid resolutions along the three Cartesian coordinate axes in the numerical calculations, although different ones can also be employed.[34]

C. Transformation of the Near Field to the Far Field in Three-Dimensional Space

In order to compute the scattering and absorption quantities, we must transform the near field obtained from the FDTD algorithm and the discrete Fourier transform technique to the far field. In the past the electromagnetic equivalence theorem has been invoked to yield the far field, from which the equivalent electric and magnetic currents are defined on a surface enclosing the particle. These currents are subsequently employed to produce the far field.[25] Such an approach, however, is not efficient in dealing with light scattering by an absorptive particle. It is well known that the absorption (σ_a), scattering (σ_s), and extinction (σ_e) cross sections of a scatterer must satisfy the energy conservation principle given by

$$\sigma_e = \sigma_s + \sigma_a . \tag{15}$$

Thus only two of the three quantities are required. According to the optical or extinction theorem,[2] one can compute the extinction cross section by using the scattering matrix value in the forward direction. If the scattering cross section rather than the absorption cross section is selected as the second independent parameter, as in the method based on the equivalence theorem, then the global distribution of the scattered energy must be integrated. For a nonspherical particle with relatively large size parameter the scattered intensity oscillates greatly in the spatial directions. For this reason one must carry out the integration of the scattered energy with a high angular resolution, which requires extremely expensive computations for randomly oriented ice crystals because the effect of the particle orientations must be averaged. To economize the computational requirement, we have developed a method to evaluate the scattered far field and the absorption cross section on the basis of the electromagnetic transformation involving a volume integration inside the particle. It should be noted that the transformation of the near field to the far field based on the volume-integration method has been used by other approaches in the frequency domain.[16–19]

The electromagnetic wave equation in the frequency domain can be written for a dielectric medium in the source-dependent form as follows:[19]

$$(\nabla^2 + k^2)\mathbf{E}(\mathbf{r}) = -4\pi(k^2\vec{\mathbf{I}} + \nabla\nabla) \cdot \mathbf{P}(\mathbf{r}), \tag{16}$$

where $\vec{\mathbf{I}}$ is a unit dyad[35] and $\mathbf{P}(\mathbf{r})$ is the polarization vector given by

$$\mathbf{P}(\mathbf{r}) = \frac{\epsilon(\mathbf{r}) - 1}{4\pi} \mathbf{E}(\mathbf{r}). \tag{17}$$

In the present investigation the dielectric medium is the scattering particle; that is, $\mathbf{P}(\mathbf{r})$ is nonzero only within the finite region inside the particle. On the basis of the vector analysis in terms of dyadic algebra[35,36] the solution for Eq. (16) is given by an integral equation in the form

$$\mathbf{E}(\mathbf{r}) = \mathbf{E}_o(\mathbf{r}) + 4\pi \int\int\int_v G(\mathbf{r}, \boldsymbol{\xi})(k^2\vec{\mathbf{I}} + \nabla_\xi\nabla_\xi) \cdot \mathbf{P}(\boldsymbol{\xi})\mathrm{d}^3\xi, \tag{18}$$

where the first term on the right-hand side is the incident wave. The domain of the integration, v, is the region inside the dielectric particle, and $G(\mathbf{r}, \boldsymbol{\xi})$ is the 3-D Green function in free space given by

$$G(\mathbf{r}, \boldsymbol{\xi}) = \frac{\exp(ik|\mathbf{r} - \boldsymbol{\xi}|)}{4\pi|\mathbf{r} - \boldsymbol{\xi}|}. \tag{19}$$

For the radiation zone or the far-field region ($kr \to \infty$) it can be proven by using Eq. (18) that the scattered or induced far field caused by the presence of the particle is

$$\mathbf{E}_s(\mathbf{r})|_{kr\to\infty} = \frac{k^2 \exp(ikr)}{4\pi r} \int\int\int_v [\epsilon(\boldsymbol{\xi}) - 1]\{\mathbf{E}(\boldsymbol{\xi}) - \hat{r}[\hat{r} \cdot \mathbf{E}(\boldsymbol{\xi})]\}\exp(-ik\hat{r} \cdot \boldsymbol{\xi})\mathrm{d}^3\xi, \tag{20}$$

where $\hat{r} = \mathbf{r}/|\mathbf{r}|$ is the unit vector in the observation direction. In order to compute the Stokes phase matrix, we need to express the scattered field given by Eq. (20) in terms of the amplitude scattering matrix. From the ge-

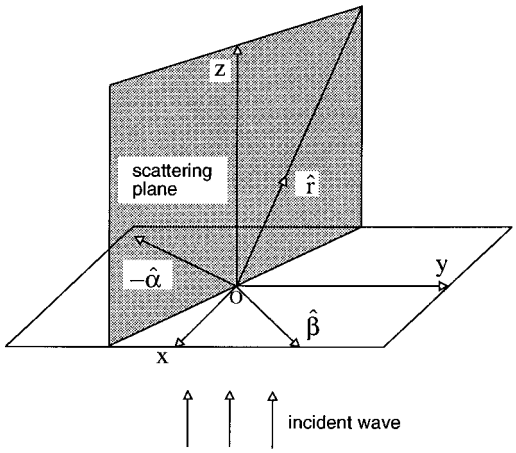

Fig. 2. Incident and scattering geometries for the transformation of the near field to the far field.

ometry defined in Fig. 2 the scattered field can be decomposed into the components parallel and perpendicular to the scattering plane in the form

$$\mathbf{E}_s(\mathbf{r}) = \hat{\alpha}E_{s,\alpha}(\mathbf{r}) + \beta E_{s,\beta}(\mathbf{r}), \tag{21}$$

where $\hat{\alpha}$ and $\hat{\beta}$ are the unit vectors parallel and perpendicular to the scattering plane, respectively, and satisfy

$$\hat{r} = \hat{\beta} \times \hat{\alpha}. \tag{22}$$

Writing Eq. (20) in a matrix form, we have

$$\begin{aligned}\begin{pmatrix} E_{s,\alpha}(\mathbf{r}) \\ E_{s,\beta}(\mathbf{r}) \end{pmatrix} &= \frac{k^2 \exp(ikr)}{4\pi r} \int\int\int_v [\epsilon(\boldsymbol{\xi}) - 1] \\ &\times \begin{pmatrix} \hat{\alpha} \cdot \mathbf{E}(\boldsymbol{\xi}) \\ \hat{\beta} \cdot \mathbf{E}(\boldsymbol{\xi}) \end{pmatrix} \exp(-ikr \cdot \boldsymbol{\xi}) \mathrm{d}^3\xi \\ &= \frac{\exp(ikr)}{-ikr} \begin{bmatrix} s_2 & s_3 \\ s_4 & s_1 \end{bmatrix} \begin{pmatrix} E_{o,\alpha} \\ E_{o,\beta} \end{pmatrix}, \end{aligned} \tag{23}$$

where s_i (i = 1 to 4) are the elements of the amplitude scattering matrix and $E_{o,\alpha}$ and $E_{o,\beta}$ are the incident E fields expressed with respect to the scattering plane. In the FDTD method the incident wave is defined with respect to the grid coordinate system $oxyz$ given by $E_{o,x}$ and $E_{o,y}$. From the geometry shown in Fig. 2 we have

$$\begin{pmatrix} E_{o,\alpha} \\ E_{o,\beta} \end{pmatrix} = \begin{bmatrix} \hat{\beta} \cdot \hat{x} & -\hat{\beta} \cdot \hat{y} \\ \hat{\beta} \cdot \hat{y} & \hat{\beta} \cdot \hat{x} \end{bmatrix} \begin{pmatrix} E_{o,y} \\ E_{o,x} \end{pmatrix}, \tag{24}$$

where $\hat{x}$ and $\hat{y}$ are unit vectors along the x and y axes, respectively. In order to obtain the scattering properties of the particle with complete polarization information, we need to select two incident cases: (1) $E_{o,x} = 1$ and $E_{o,y} = 0$ and (2) $E_{o,x} = 0$ and $E_{o,y} = 1$. With these selections we can define the following quantities:

$$\begin{aligned}\begin{pmatrix} F_{\alpha,x} \\ F_{\beta,x} \end{pmatrix} &= \frac{ik^3}{4\pi} \int\int\int_v [1 - \epsilon(\boldsymbol{\xi})] \begin{pmatrix} \hat{\alpha} \cdot \mathbf{E}(\boldsymbol{\xi}) \\ \hat{\beta} \cdot \mathbf{E}(\boldsymbol{\xi}) \end{pmatrix} \\ &\times \exp(-ik\hat{r} \cdot \boldsymbol{\xi}) \mathrm{d}^3\xi \Big|_{E_{o,x}=1, E_{o,y}=0}, \end{aligned} \tag{25a}$$

$$\begin{aligned}\begin{pmatrix} F_{\alpha,y} \\ F_{\beta,y} \end{pmatrix} &= \frac{ik^3}{4\pi} \int\int\int_v [1 - \epsilon(\boldsymbol{\xi})] \begin{pmatrix} \hat{\alpha} \cdot \mathbf{E}(\boldsymbol{\xi}) \\ \hat{\beta} \cdot \mathbf{E}(\boldsymbol{\xi}) \end{pmatrix} \\ &\times \exp(-ikr \cdot \boldsymbol{\xi}) \mathrm{d}^3\xi \Big|_{E_{o,x}=0, E_{o,y}=1}. \end{aligned} \tag{25b}$$

Using Eqs. (23)–(25) along with some algebraic manipulations, one can prove that

$$\begin{bmatrix} s_2 & s_3 \\ s_4 & s_1 \end{bmatrix} = \begin{bmatrix} F_{\alpha,y} & F_{\alpha,x} \\ F_{\beta,y} & F_{\beta,x} \end{bmatrix} \begin{bmatrix} \hat{\beta} \cdot \hat{x} & \hat{\beta} \cdot \hat{y} \\ -\hat{\beta} \cdot \hat{y} & \beta \cdot \hat{x} \end{bmatrix}. \tag{26}$$

After the amplitude scattering matrix is defined, the corresponding Stokes phase matrix can be determined and numerically computed. It should be noted that for ice crystals randomly oriented in space there are only six independent nonzero elements for the 4×4 phase matrix.[2]

To derive the integral equations for the absorption and extinction cross sections, we start from the Maxwell equations. For a nonferromagnetic dielectric medium with an incident harmonic wave whose time dependence is given by $\exp(-i\omega t)$ the Maxwell curl equations in the frequency domain can be written in the forms

$$c\nabla \times \mathbf{H} = -i\omega(\epsilon_r + i\epsilon_i)\mathbf{E}, \tag{27a}$$

$$c\nabla \times \mathbf{E} = i\omega\mathbf{H}. \tag{27b}$$

Using these equations along with the vector algebra, we obtain

$$-\nabla \cdot \mathbf{s} = \frac{i\omega}{4\pi}(\epsilon_r \mathbf{E} \cdot \mathbf{E}^* - \mathbf{H} \cdot \mathbf{H}^*) + \frac{\omega\epsilon_i}{4\pi} \mathbf{E} \cdot \mathbf{E}^*, \tag{28a}$$

$$\mathbf{s} = \frac{c}{4\pi} \mathbf{E} \times \mathbf{H}^*, \tag{28b}$$

where an asterisk denotes the complex conjugate and $\mathbf{s}$ is a complex Poynting vector for the electromagnetic wave. Taking the real part of Eq. (28a) and integrating it over the region inside the scattering particle leads to

$$\begin{aligned} -\mathrm{Re}\left[\int\int\int_v \nabla \cdot \mathbf{s}(\boldsymbol{\xi}) \mathrm{d}^3\xi\right] &= -\mathrm{Re}\left[\oiint \hat{n} \cdot \mathbf{s}(\boldsymbol{\xi}) \mathrm{d}^2\xi\right] \\ &= \frac{\omega}{4\pi} \int\int\int_v \epsilon_i \mathbf{E}(\boldsymbol{\xi}) \\ &\cdot \mathbf{E}^*(\boldsymbol{\xi}) \mathrm{d}^3\xi, \end{aligned} \tag{29}$$

where $\hat{n}$ is the outward-pointing unit vector normal to the particle surface. According to the physical meaning of the Poynting vector,[37] the surface-integration term in Eq. (29) is the net rate at which electromagnetic energy penetrates into the particle surface, that is, the energy absorbed by the particle. Further, the incident electromagnetic flux is given by

$$F_o = \frac{c}{4\pi} \mathbf{E}_o \cdot \mathbf{E}_o^* = \frac{c}{4\pi} |\mathbf{E}_o|^2. \tag{30}$$

Thus the absorption cross section of the particle can then be expressed by

$$\sigma_a = -\mathrm{Re}\left[\oiint \hat{n} \cdot \mathbf{s}(\boldsymbol{\xi})\mathrm{d}^2\xi \right] \Big/ F_o$$

$$= \frac{k}{|\mathbf{E}_o|^2} \int\int\int_v \epsilon_i(\boldsymbol{\xi})\mathbf{E}(\boldsymbol{\xi}) \cdot \mathbf{E}^*(\boldsymbol{\xi})\mathrm{d}^3\xi. \quad (31)$$

In conjunction with the derivation of the extinction cross section we note that the Poynting vector can be decomposed into incident, scattered, and extinction components as follows:

$$\mathbf{s} = \mathbf{s}_e + \mathbf{s}_s + \mathbf{s}_i . \quad (32)$$

The complex extinction component of the Poynting vector is given by

$$\mathbf{s}_e = \frac{c}{4\pi} (\mathbf{E}_o \times \mathbf{H}^* + \mathbf{E}^* \times \mathbf{H}_o). \quad (33)$$

Using Eqs. (27) and (33), we can prove that the electromagnetic energy associated with the extinction is given by

$$-\mathrm{Re}\left[\oiint \hat{n} \cdot \mathbf{s}_e(\boldsymbol{\xi})\mathrm{d}^2\xi \right]$$

$$= \frac{\omega}{4\pi} \mathrm{Im}\left\{ \int\int\int_v [\epsilon(\boldsymbol{\xi}) - 1]\mathbf{E}(\boldsymbol{\xi}) \cdot \mathbf{E}^*(\boldsymbol{\xi})\mathrm{d}^3\xi \right\}. \quad (34)$$

Consequently, the extinction cross section can be obtained from

$$\sigma_e = \frac{\omega}{4\pi} \mathrm{Im}\left\{ \int\int\int_v [\epsilon(\boldsymbol{\xi}) - 1]\mathbf{E}(\boldsymbol{\xi}) \cdot \mathbf{E}^*(\boldsymbol{\xi})\mathrm{d}^3\xi \right\} \Big/ F_o$$

$$= \mathrm{Im}\left\{ \frac{k}{|\mathbf{E}_o|^2} \int\int\int_v [\epsilon(\mathbf{r}) - 1]\mathbf{E}(\boldsymbol{\xi}) \cdot \mathbf{E}_o^*(\boldsymbol{\xi})\mathrm{d}^3\xi \right\}. \quad (35)$$

Thus, if the electric field inside the particle is given, the scattered far field and various cross sections can be determined from Eqs. (25), (26), (31), and (35). Also, the electric field inside the particle can be obtained by using the preceding FDTD method.

For the scattering by a nonspherical particle the absorption and extinction cross sections depend on the polarization of the incident wave. However, if the mean values of the cross section (average of the cross sections with respect to the two perpendicularly polarized incident waves) are considered, they are independent of the plane on which the polarization of the incident wave is defined. Using Eqs. (23) and (35) along with integration by parts, we can prove that the mean extinction cross section is

$$\bar{\sigma}_e = (\sigma_{e,\parallel} + \sigma_{e,\perp})/2$$

$$= \frac{2\pi}{k^2} \mathrm{Re}[s_1(\hat{z}) + s_2(\hat{z})]. \quad (36)$$

The above equation actually is a particular form of the optical or extinction theorem. Similarly, the mean absorption cross section is also independent of the scattering plane and can be computed by using Eq. (31) with respect to the two incident cases.

3. NUMERICAL RESULTS AND DISCUSSIONS

A. Validation of the Finite-Difference Time Domain Method in Three-Dimensional Space

The accuracy of the FDTD method has been comprehensively checked with Mie results for metal objects by a number of researchers.[38] However, its accuracy has not been verified for randomly oriented ice particles. In our previous study for the 2-D scattering problem a fine grid size ($\Delta = \lambda/60$) was used. Such a fine grid size, however, will require considerable computer time and memory in the 3-D case. In order to optimize numerical calculations and to investigate the effect of the grid size on the accuracy of the FDTD results, we have selected three grid sizes of $\Delta s = \lambda/10$, $\lambda/20$, and $\lambda/30$ in comparison with the exact Mie results for the scattering of light by ice spheres. Since the FDTD method does not pose a preferential treatment to any geometry (with the possible exception of rectangular objects in a Cartesian grid), the solution for spheres constitutes a representative test of the accuracy of the FDTD method. Moreover, the objective of our study is for ice crystals. Thus we have chosen two representative refractive indices for ice at the visible (0.55-μm) and thermal infrared (10.8-μm) wavelengths at which negligible and strong absorption are involved.

Figure 3 shows comparisons of the phase function computed by the FDTD method and by Mie theory for the size parameter $ka = 5$ at $\lambda = 0.55$ and 10.8 μm. Deviations of the FDTD results from the exact Mie solutions are presented in terms of the absolute error, P_{11}(FDTD) $- P_{11}$(Mie), as well as the relative error, $[P_{11}$(FDTD) $- P_{11}$(Mie)$]/P_{11}$(Mie). Errors in the FDTD results are produced by the numerical dispersion of the finite-difference analog, the approximation of a sphere by a pseudosphere constructed by cubic grid cells (staircasing effect), and the representation of the near field by the discretized data that do not account for the field variation within each cell, all of which are associated with the grid size used in the calculations. Compared with the Mie theory, the FDTD method with a grid size of $\Delta s = \lambda/10$ can produce significant errors in the phase function for both nonabsorptive and absorptive wavelengths. Errors in the FDTD results, however, decrease significantly as the grid size is reduced to $\Delta s = \lambda/20$ and $\lambda/30$. In both cases the FDTD results for the phase function essentially converge to the Mie solutions. The results for the three other phase matrix elements, not shown here, are similar to those for the phase function.

Figure 4 shows comparisons of the nonzero elements of the phase matrix computed by the FDTD technique and by Mie theory for the size parameter $ka = 15$ at the 0.55-μm wavelength. Differences between the FDTD and Mie results for the phase matrix elements associated with the polarization configuration are presented only in terms of the absolute errors. This is because the definition of the relative errors is not meaningful when the quantities are 0 or approaching 0. For the phase function the maximum absolute errors are noted in the forward direction. However, maximum relative errors are seen at the scattering angle of 135° and backscattering directions. The error peak at 135° is associated with the

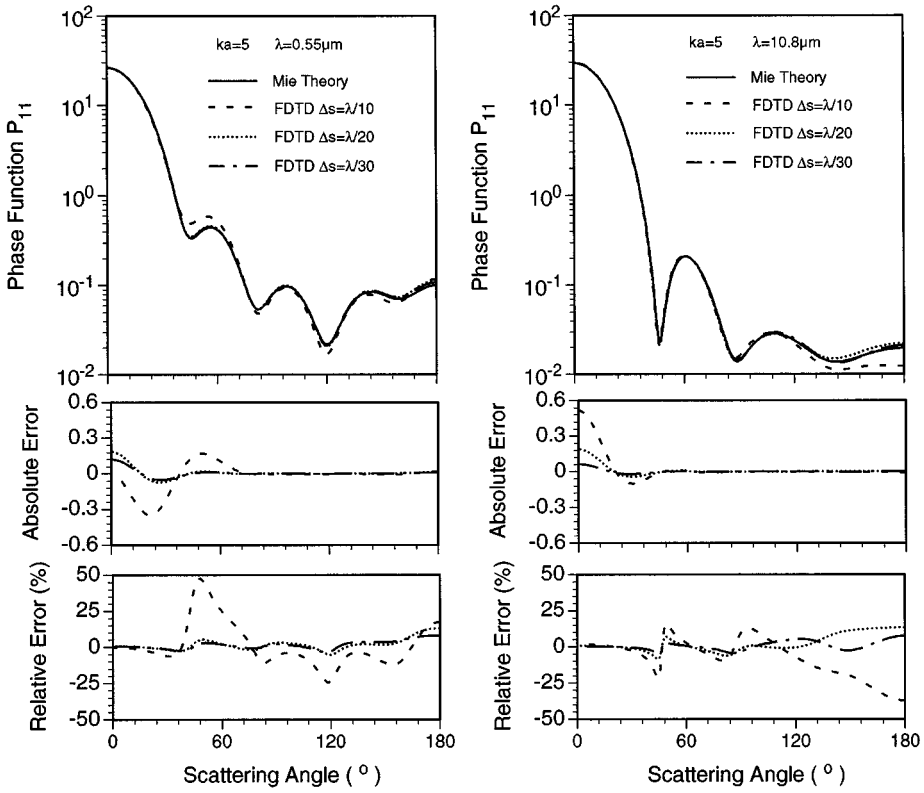

Fig. 3. Comparison of the phase function computed by the FDTD method and by Mie theory for the size parameter ka of 5 at $\lambda = 0.55$ and 10.8 μm in terms of absolute and relative errors. The indices of refraction for ice at these wavelengths are $1.311 + i3.11 \times 10^{-9}$ and $1.0893 + i0.18216$. Three grid sizes are used in the FDTD calculations.

artificial reflection that is due to the imperfect absorbing boundary condition applied to the outer boundary of the computation domain. The maximum spurious reflection from the corners and the edges of the grid mesh will cause a detectable error in the region near the 135° scattering direction, where the scattered energy is small. The second maximum near backscattering is associated with a small amount of residual energy that remains inside the particle when the time-marching iteration to compute the near field is terminated. This small amount of energy cannot be accounted for in the transformation of the near field from the time domain to the frequency domain by a discrete Fourier transform, leading to an underestimation of the scattered energy when the far field is calculated on the basis of the near field in the frequency domain. As stated in Subsection 2.A and discussed in our previous study,[11] with the initial excitation using a pulse source, the convergence for the near-field computation requires that the field in the time domain reduce to 0. In our computations the number of time-marching iterations is $50N_m$, where N_m is the grid number along the maximum dimension of the computational domain. However, the temporal duration over which the near field decays essentially to 0 is proportional to the particle size in a nonlinear way. In the case of $ka = 15$ a few percent of the incident energy still remains inside the particle when the time-marching iteration is terminated, and it is not accounted for when the field in the frequency domain is computed. Underestimation of a few percent will impact the accuracy in computing the side and backward scattering, where the scattered intensity is much smaller than the forward-scattered intensity. In this case relative errors can be potentially large. The residual energy discussed above corresponds to the high-order multipole radiation in the frequency domain and converges very slowly. We find that the CPU time must be increased by a factor of 2–3 in order to converge the residual energy to less than 1% for $ka = 5$. For $ka = 15$ we anticipate a substantial increase in the computational effort, although numerical experiments have not been carried out in this case because the enormous computer time required is beyond the resources available to us.

Comparing Figs. 3 and 4, we see that the accuracy of the FDTD method depends not only on the grid size but also on the size of the scattering object. The overall agreement of the FDTD and Mie results for $ka = 15$ appears reasonable when the grid size of $\lambda/20$ is used. To run this case, we have used approximately 10 h on the Cray Y-MP computer. It is quite clear that in order to produce reliable results for size parameters larger than approximately 15 with the FDTD method, one must use significant computer time.

Figure 5 shows the extinction and absorption efficiencies computed by the FDTD method and by Mie theory. Also shown are the differences in terms of absolute and relative errors. Since the absorption efficiency at the 0.55-μm wavelength is negligible, the absorption efficiency is not plotted. When $\Delta s = \lambda/10$ is used, significant errors can be noted at both wavelengths for size parameters larger than 5. For $ka = 10$ an $\sim -12\%$ error is

noted for the extinction efficiency at $\lambda=0.55$ μm, while $\sim -17\%$ and $\sim -16\%$ are noted for the extinction and absorption efficiencies, respectively, at $\lambda = 10.8$ μm. When the grid size decreases to $\Delta s = \lambda/20$ and $\lambda/30$, errors reduce drastically. From Fig. 5 we also note that the relative error at $ka = 0.2$ is even larger than that at $ka = 1$ and 3. This is because only a few grid cells are used to approximate the sphere when it is very small. Furthermore, the roughness of the surface for the pseudosphere in comparison with its radius is relatively larger in the case of $ka = 0.2$ than for $ka = 1$ and 3. Thus, for a very small particle, one should use small grid sizes in order to reduce the inaccuracy caused by the staircasing effect. Implementation of the fine grid size will not significantly increase the computational burden for very small particles. The results shown in Fig. 5 reveal that errors decrease with decreasing grid size but increase with increasing particle size. For size parameters smaller than 3 a very coarse grid ($\Delta s \sim \lambda/10$) can be used to produce reasonable accuracy. However, for $ka > 5$, the grid size must be smaller than $\sim\lambda/20$ in order to produce reliable results.

From Figs. 3–5 it is evident that the grid size is the dominating factor in determining the numerical errors associated with the FDTD technique. According to the preceding comparisons, we conclude that the overall agreement between the FDTD results and the Mie solutions is excellent for size parameters less than approximately 15 if the grid size of $\Delta s = \lambda/20$ or $\lambda/30$ is used. Formidable computer time is required to produce reliable results for size parameters larger than approximately 15 if the FDTD method is used for the solution of light scattering by spheres.

B. Finite-Difference Time Domain Method for Light Scattering by Hexagonal Ice Crystals

In this subsection we apply the FDTD method to investigate the scattering characteristics of hexagonal ice crystals with specific and random orientations in 3-D space. The orientation of the symmetric hexagonal ice crystal with respect to the incident wave can be specified by the elevation of the c axis (symmetric axis) and the rotational angle around this axis, which ranges from 0° to 90° and 0° to 30°, respectively. We find that 5° and 3° are sufficient

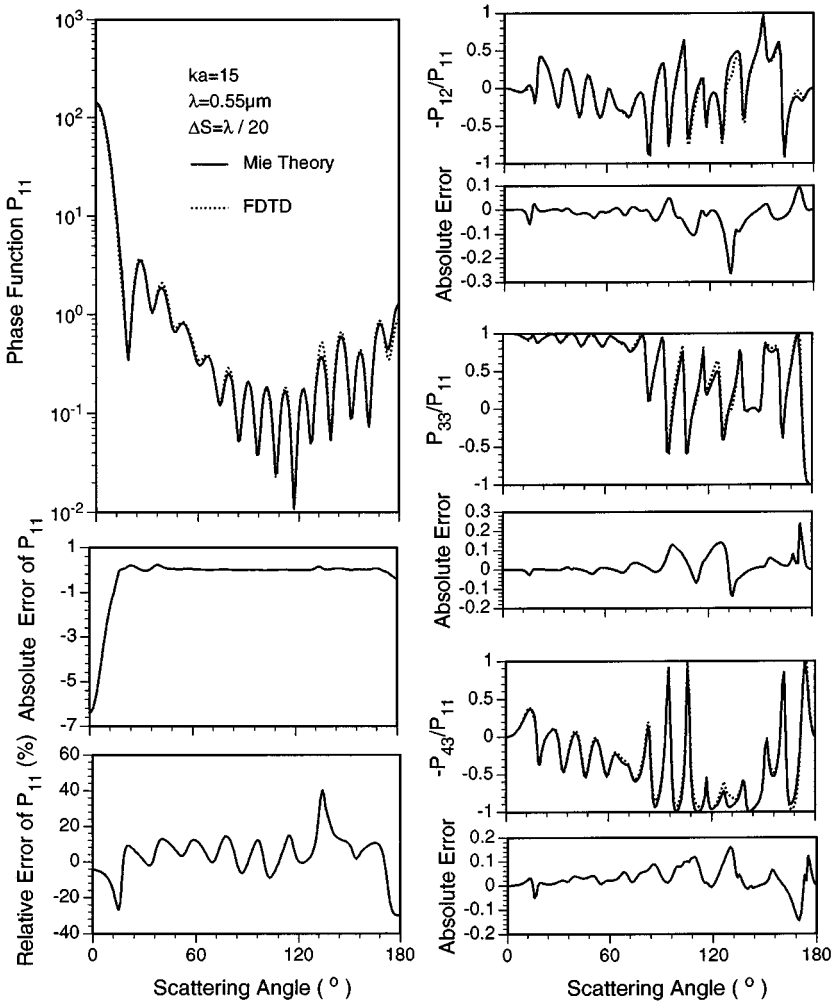

Fig. 4. Comparison of the phase matrix elements computed by the FDTD method and by Mie theory for the size parameter of 15 at $\lambda = 0.55$ μm. The grid size used is $\lambda/20$, and errors produced by the FDTD technique are also presented for this larger size parameter (see the text for further discussion).

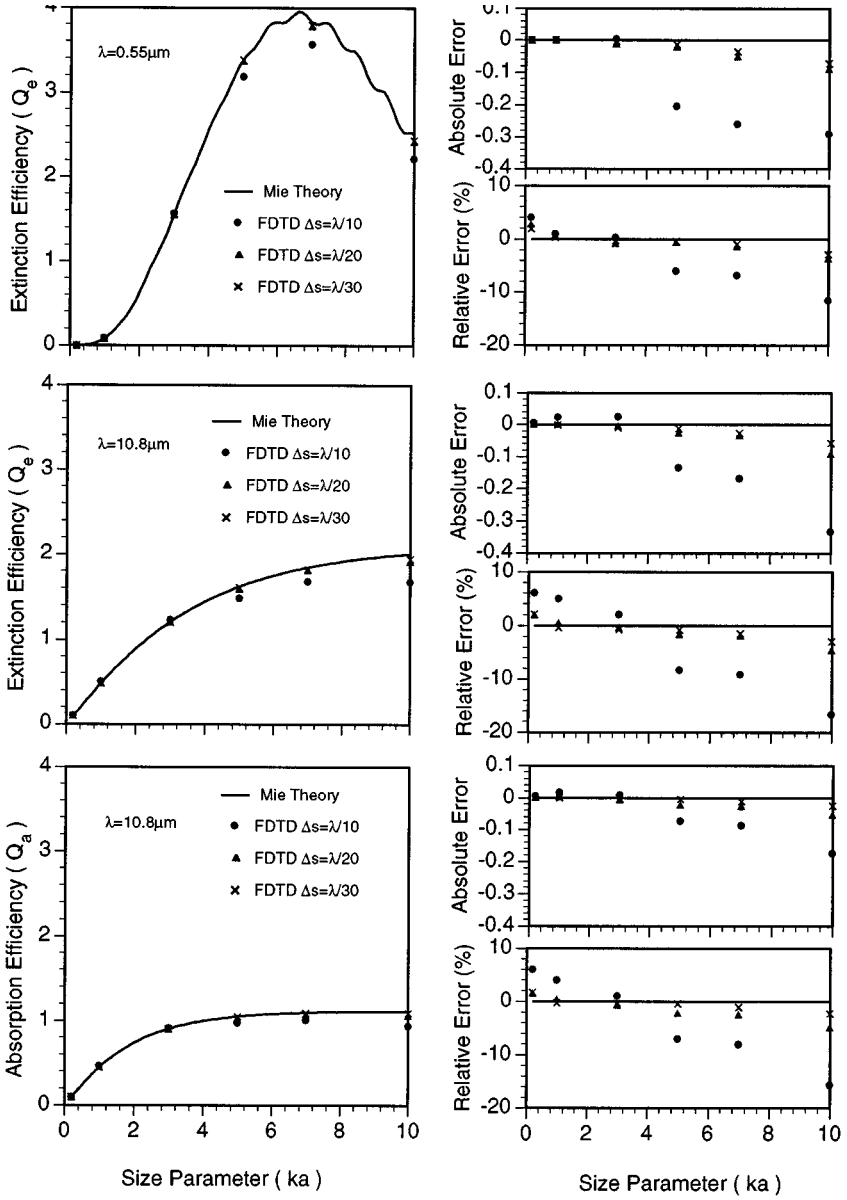

Fig. 5. Extinction and absorbing efficiencies for ice spheres as functions of size parameter computed by the FDTD method and by Mie theory at $\lambda = 0.55$ and 10.8 μm. Also shown are the absolute and relative differences between the two results.

angular intervals in the average of these two angles. The average of the scattered intensity over the azimuthal angle in our calculations was made by an angular resolution of 2° after considerable numerical experimentation to produce an optimized value. It should be noted that small ice crystals in the Earth's atmosphere tend to be randomly oriented. The results presented below are intended to be representative rather than extensive.

Figure 6 shows the phase function and the degree of linear polarization of a hexagonal column for $\lambda = 0.55$ μm with two specified incident configurations, as shown in the plots. In this figure L and a denote the length and the half-width of a column crystal, respectively. With a specific orientation the scattering characteristics of ice crystals depend not only on the zenith angle but also on the azimuthal angle with respect to the scattering direction. The results are azimuthally averaged, viz.,

$$P(\theta) = \frac{1}{2\pi}\int_0^{2\pi} P(\theta, \phi)\mathrm{d}\phi. \tag{37}$$

The scattering parameters depend significantly on the particle orientation with respect to the incident direction. The scattering cross section of an ice column with end-facing incidence is approximately 2.5 times larger than that with side-facing incidence. When the incident direction is perpendicular to the symmetric axis of the ice column, the scattered field is dominated by dipole radiation because the scattering capacity of the particle is very small. Thus oscillation does not occur in the phase function, and the scattering pattern is similar to Rayleigh scattering, with a broad minimum occurring at the 90° scattering angle. When the incident direction is toward the end of the particle, the scattering capacity increases

because of the significant contribution of higher-order terms in the multipole expansion of the scattered field. The phase interference becomes important for the induced radiation from different parts of the particle, leading to the ripple structure in both phase function and polarization.

Figure 7 shows the nonzero elements of the phase matrix for randomly oriented ice columns at two wavelengths: 0.55 and 3.7 μm. After averaging over all orientations of the ice crystals, the phase matrix is independent of the azimuthal angle of the scattering plane. The results for these two wavelengths are similar for the following reason. Absorption is approximately proportional to the particle volume, so that its effect at the 3.7-μm wavelength is not significant for small size parameters in the determination of the angular distribution of the scattered energy and polarization. The element $-P_{12}/P_{11}$, the degree of linear polarization, for randomly oriented ice crystals is positive in the middle scattering angle region, in agreement with the conclusion presented by Asano and Sato,[39] who noted that the linear polarization of light scattered by nonspherical particles, in contrast to that scattered by spheres, tends to be positive in these scattering angles. The matrix elements P_{22}/P_{11} are 1 for spheres. Thus the departure of P_{22}/P_{11} from 1 can be used as a measure of nonsphericity. It should be pointed out that the present results are for small finite hexagonal ice crystals in both width and length. For this reason the phase functions do not display 22° and 46° halo peaks, produced by the geometric optics approach. A maximum at the 150° scattering angle is noted, however.

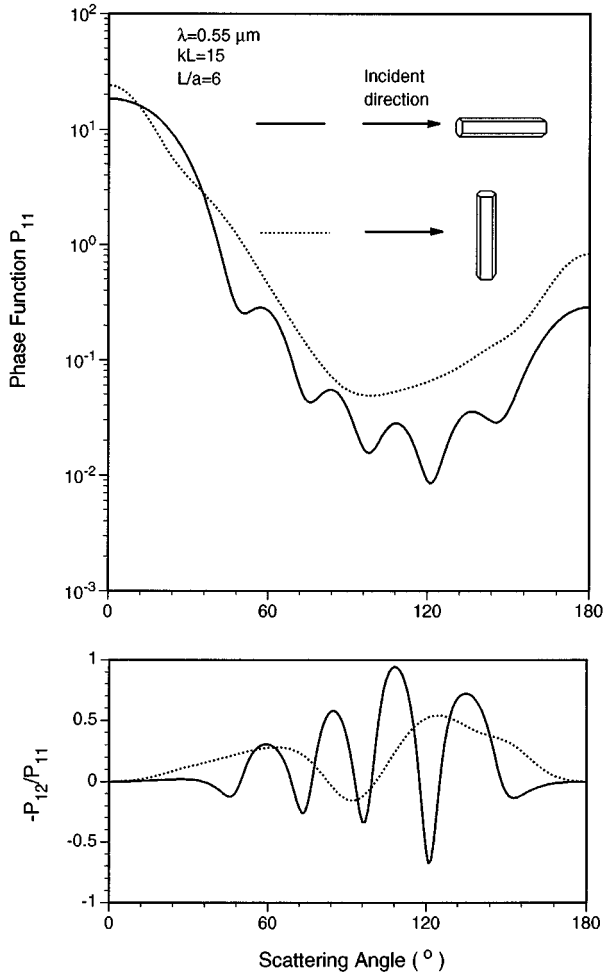

Fig. 6. Phase functions and degrees of linear polarization computed by the FDTD method for hexagonal ice columns with two specified orientations at $\lambda = 0.55$ μm. L is the length of the ice column, and a is the half-width.

Shown in Fig. 8 are the extinction efficiencies computed by the FDTD method for randomly oriented hexagonal ice crystals. Also shown are the results for the equivalent-volume and -surface spheres. The equivalent-surface spheres have the same cross-sectional area perpendicular to the incident direction as that of the randomly oriented hexagons. Replacement of the small hexagonal ice crystals by both equivalent spheres significantly overestimates the extinction efficiency, revealing that the shape effect is significant for small size parameters. From Fig. 8 we also see that deviations produced by the equivalent-volume sphere approximation are less because the induced radiation by the polarized dipole inside the particle, which contributes significantly to the scattered field for small size parameters, is proportional to the particle volume.

Comparisons of the phase functions computed by the FDTD technique and by the conventional ray-tracing method for randomly oriented ice crystals are presented in Fig. 9 for $kL = 20$ (equivalent to $ka = 10$). For the case of $L/a = 6$, because of the small cross section for ice columns the higher-order multipole radiation is insignificant. The scattering peaks corresponding to halo features are not observable in the phase function. For the case of $L/a = 2$, where the cross section for ice plates is increased by a factor of 3, a pronounced scattering maximum at the 22° scattering angle is generated in the FDTD solution. We estimate that when the ice crystal size parameter is smaller than approximately 20 in terms of either length or diameter, the halo peaks cannot be produced. To demonstrate the flexibility of the FDTD technique for application to the scattering of light by irregularly shaped ice crystals, we compute the phase function for bullet rosettes and hollow columns. The results are also presented in Fig. 9. Comparisons are made with the results computed by using the Monte Carlo/geometric ray-tracing method developed by Takano and Liou.[40] The cross angle for the bullets is 90°, the tip length of a bullet is t, the depth of the hollow pyramid is denoted by d, and the other parameters defining the geometry of the ice crystals are given in the figure. Significant deviations of the phase functions for bullet rosettes given by the two methods are found for scattering angles less than ~12°. In addition, significant errors of the geometric optics solution are noted near the backscattering direction. For the case of hollow columns significant errors are noted for scattering angles smaller than 20° and larger than 30°. Similar to the hexagonal case of $L/a = 6$, scattering peaks corresponding to halos are not displayed in the FDTD results because the size parameter is too small. From Fig. 9 we note that the geometric optics method considerably overestimates the backscattering for small size parameters for both hexagonal and bullet rosette shapes.

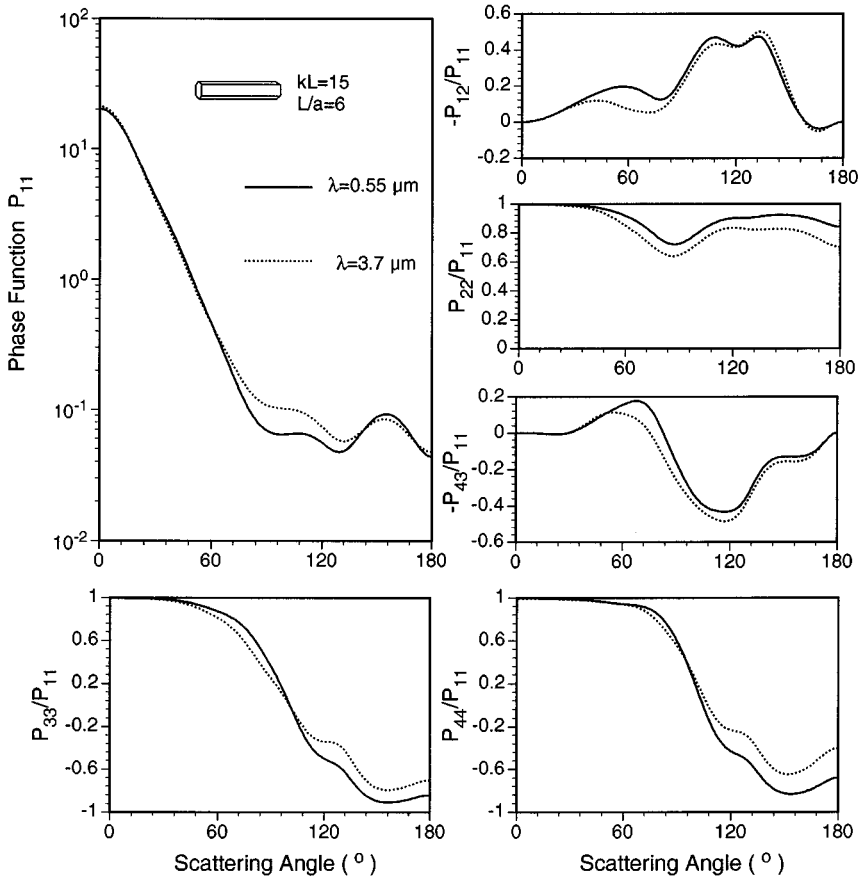

Fig. 7. Nonzero elements of the phase matrix computed by the FDTD method at two wavelengths, 0.55 and 3.7 μm (m = 1.4005 + i7.1967 × 10^{-3}), for randomly oriented hexagonal columns.

Overall, the conventional geometric ray-tracing technique is inadequate in producing reliable phase function and polarization patterns for size parameters smaller than ~30–40.

4. CONCLUSIONS

We have extended the FDTD technique developed for a 2-D scattering problem to the general 3-D counterpart. In this extension we have introduced a new way of defining the effective permittivity and conductivity to transform the basic Maxwell equations to a source-dependent form that governs the scattering process of a dielectric particle so that the complex calculations can be avoided when the scatterer is absorptive. Another new endeavor includes the derivation of the finite-difference analog of the transformed Maxwell equations in terms of the total-field algorithm in which the connecting conditions are given explicitly for applying the absorbing boundary condition in the algorithm. We have also applied an integral technique to compute the far field and the extinction and absorption cross sections so as to avoid the high-resolution requirement in the angular integration of the scattered energy in determining the scattering cross section, which has been done conventionally by a surface-integration technique.

The accuracy of the FDTD results in 3-D space is

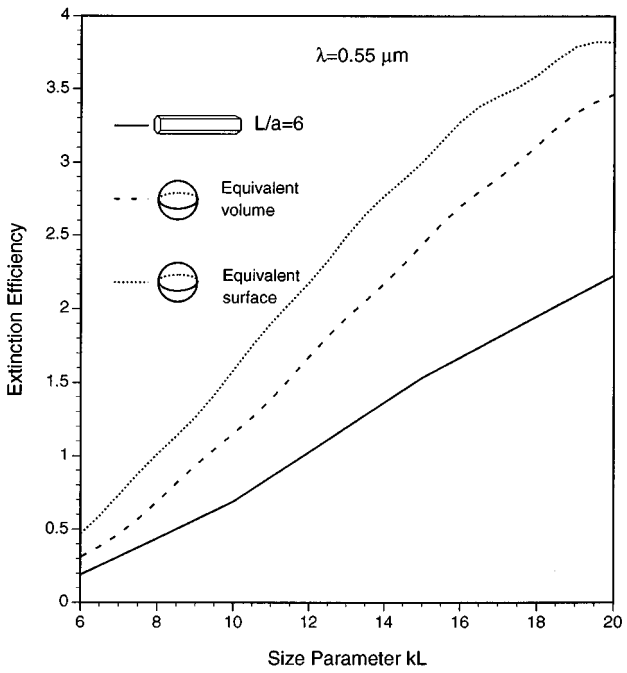

Fig. 8. Extinction efficiencies of randomly oriented hexagonal ice crystals computed by the FDTD method and by the Mie theory for equivalent-volume and -surface spheres.

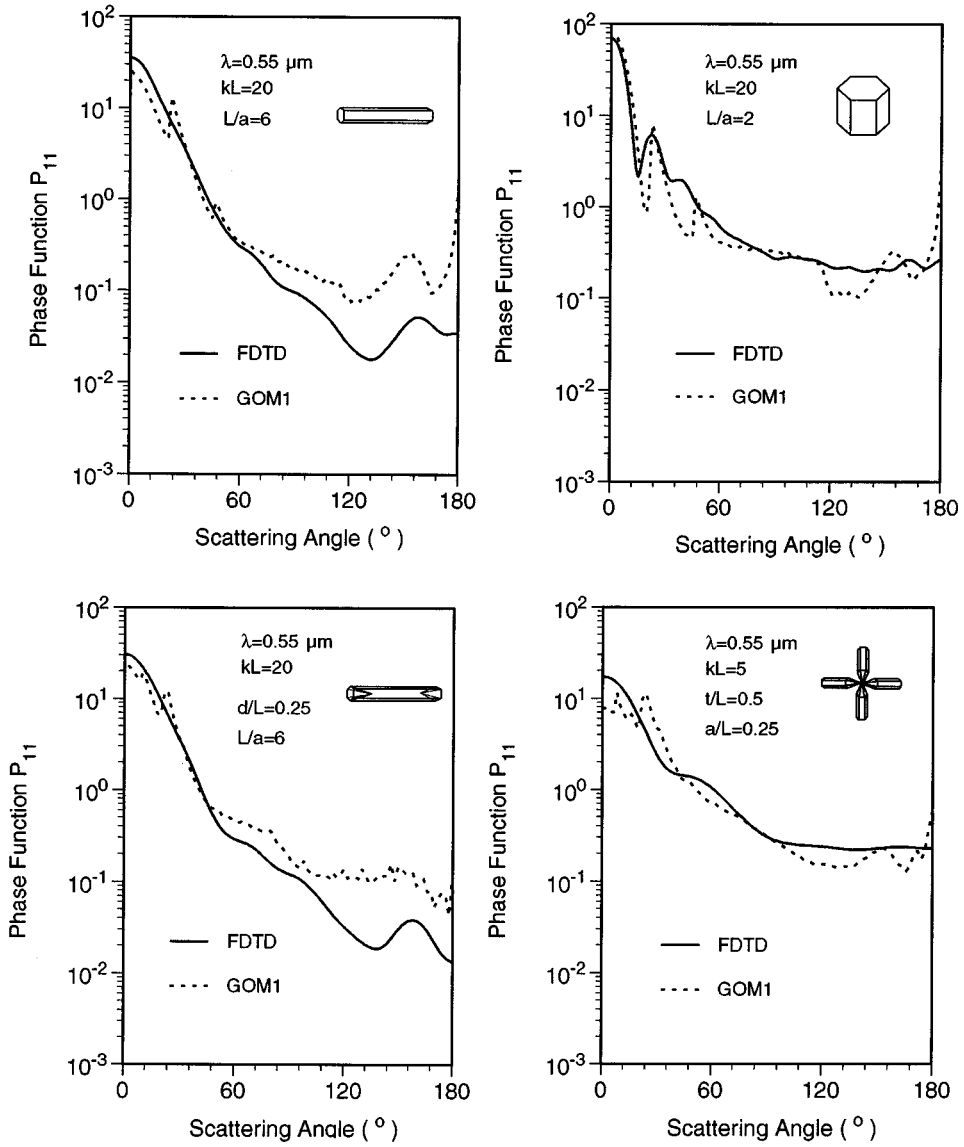

Fig. 9. Comparison of phase functions for hexagonal ice crystals computed by the FDTD method and by a geometric ray-tracing method (GOM1) for solid and hollow columns, plates, and bullet rosettes.

checked with the results computed by the exact Mie theory for spheres. We show that the FDTD technique is an accurate and efficient method for size parameters less than approximately 10–20, above which considerable computer time is required. It becomes less accurate for size parameters larger than approximately 20 because of the numerical approximation of the particle shape and the limitation of the absorbing boundary condition imposed.

The FDTD method is applied to the calculation of the phase matrix and the extinction and absorption cross sections for ice crystals with size parameters less than 20. Specific and random orientations for columns and plates are used in the calculations. We illustrate that the scattering patterns for small hexagonal ice crystals in terms of phase function, polarization, and extinction efficiency differ from those for large ice crystals and spheres. In particular, we show that the geometric ray-tracing method is not suitable for computing the phase function for hexagonal ice crystals with size parameters less than 20 and that the approximation using equivalent spheres (in terms of either volume or surface) for small ice crystals leads to significant errors.

We also demonstrate that the FDTD method can be effectively applied to hollow columns and bullet rosettes, two types of irregular ice crystal that frequently occur in cirrus clouds. The application requires only the geometric definition of the irregular ice crystal shape, and no additional computational effort is needed. The FDTD technique is thus an attractive numerical method for the solution of light scattering and absorption by small irregular particles (aerosols and ice crystals) with defined geometries and known optical properties.

ACKNOWLEDGMENTS

This study was supported by National Science Foundation (NSF) grant ATM-93-1521 and in part by NASA grant NAG1-1719 and U.S. Department of Energy grant DE-FG03-95ER 61991. Most of the computational results presented in this paper were obtained from the use of the Cray Y-MP 8/864 at the National Center for Atmospheric Research, which is sponsored by the NSF.

Address all correspondence to K. N. Liou: telephone, 801-581-3336; fax, 801-581-4065; e-mail, knliou@climate.utah.edu.

REFERENCES

1. G. Mie, "Beitrage zur Optik truber Medien speziell kolloidaler Metallosungen,"Ann. Phys. (Leipzig) **25**, 377–445 (1908).
2. H. C. van de Hulst, *Light Scattering by Small Particles* (Wiley, New York, 1957).
3. M. Kerker, D. Cooke, W. A. Farone, and R. T. Jacobsen, "Electromagnetic scattering from an infinite circular cylinder at oblique incidence. I. Radiance functions for $m = 1.46$," J. Opt. Soc. Am. **56**, 487–491 (1966).
4. K. N. Liou, "Light scattering by ice clouds in the visible and infrared: a theoretical study," J. Atmos. Sci. **29**, 524–536 (1972).
5. S. Asano and G. Yamamoto, "Light scattering by a spheroidal particle," Appl. Opt. **14**, 29–49 (1975).
6. S. Asano, "Light scattering properties of spheroidal particle," Appl. Opt. **18**, 712–723 (1979).
7. Q. Cai and K. N. Liou, "Polarized light scattering by hexagonal ice crystals: theory," Appl. Opt. **21**, 3569–3580 (1982).
8. Y. Takano and K. N. Liou, "Solar radiation transfer in cirrus clouds. Part I. Single-scattering and optical properties of hexagonal ice crystals," J. Atmos. Sci. **46**, 3–19 (1989).
9. K. Muinonen, "Scattering of light by crystals: a modified Kirchhoff approximation," Appl. Opt. **28**, 3044–3050 (1989).
10. A. Macke, "Scattering of light by polyhedral ice crystals," Appl. Opt. **32**, 2780–2788 (1993).
11. P. Yang and K. N. Liou, "Light scattering by hexagonal ice crystals: comparison of finite-difference time domain and geometric optics models," J. Opt. Soc. Am. A **12**, 162–176 (1995).
12. Lord Rayleigh, "On the light from the sky, its polarization and colour," Philos. Mag. **41**, 107–120, 274–279 (1871) [reprinted in *Scientific Papers by Lord Rayleigh, Vol. I: 1869–1881, No. 8* (Dover, New York, 1964)].
13. P. W. Barber and C. Yeh, "Scattering of electromagnetic waves by arbitrarily shaped dielectric bodies," Appl. Opt. **14**, 2864–2872 (1975).
14. R. F. Harrington, *Field Computation by Moment Methods* (Macmillan, New York, 1968).
15. M. A. Morgan, "Finite element calculation of microwave absorption by the cranial structure," IEEE Trans. Biomed. Eng. **BME-28**, 687–695 (1981).
16. E. M. Purcell and C. P. Pennypacker, "Scattering and absorption of light by nonspherical dielectric grains," Astrophys. J. **196**, 705–714 (1973).
17. P. J. Flatau, G. L. Stephens, and B. T. Draine, "Light scattering by rectangular solids in the discrete-dipole approximation: a new algorithm exploiting the block-toeplitz structure," J. Opt. Soc. Am. A **7**, 593–600 (1990).
18. B. T. Draine and P. J. Flatau, "Discrete-dipole approximation for calculations," J. Opt. Soc. Am. A **11**, 1491–1499 (1994).
19. G. H. Goedecke and S. G. O'Brien, "Scattering by irregular inhomogeneous particles via the digitized Green's function algorithm," Appl. Opt. **15**, 2431–2437 (1988).
20. H. Y. Chen and M. F. Iskander, "Light scattering and absorption by fractal agglomerate and coagulations of smoke aerosols," J. Mod. Opt. **37**, 171–181 (1990).
21. P. C. Waterman, "Matrix formulation of electromagnetic scattering," Proc. IEEE **53**, 805–812 (1965).
22. P. W. Barber and S. C. Hill, *Light Scattering by Particles: Computational Methods* (World Scientific, Singapore, 1990).
23. P. Chiappetta, "Multiple scattering approach to light scattering by arbitrarily shaped particles," J. Phys. A **13**, 2101–2108 (1980).
24. S. K. Yee, "Numerical solution of initial boundary value problems involving Maxwell's equation in isotropic media," IEEE Trans. Antennas Propag. **AP-14**, 302–307 (1966).
25. K. Umashankar and A. Taflove, "A novel method to analyze electromagnetic scattering of complex objects," IEEE Trans. Electromagn. Compat. **EMC-24**, 397–405 (1982).
26. K. S. Kunz and R. J. Luebbers, *The Finite Difference Method for Electromagnetics* (CRC Press, Boca Raton, Fla., 1993).
27. A. Taflove, *Computational Electrodynamics in the Finite-Difference Time Domain Method* (Artech House, Boston, Mass., 1995).
28. G. Mur, "Absorbing boundary conditions for the finite-difference approximation of the time-domain electromagnetic-field equations," IEEE Trans. Electromagn. Compat. **EMC-23**, 377–382 (1982).
29. Z. Liao, H. L. Wang, B. Yang, and Y. Yuan, "A transmitting boundary for transient wave analyses," Sci. Sin. **27**, 1063–1076 (1984).
30. W. C. Chew and W. H. Weedon, "A 3D perfectly matched medium from modified Maxwell's equations with stretched coordinates," Microwave Opt. Tech. Lett. **7**, 599–604 (1994).
31. K. L. Shlager, J. G. Maloney, S. L. Ray, and A. F. Peterson, "Relative accuracy of several finite-difference time-domain methods in two and three dimensions," IEEE Trans. Antennas Propag. **41**, 1732–1737 (1993).
32. S. A. Schelkunoff, *Electromagnetic Waves* (Van Nostrand, New York, 1943).
33. D. E. Merewether, R. Fisher, and F. W. Smith, "On implementing a numeric Huygens's source in a finite difference program to illuminate scattering bodies," IEEE Trans. Nucl. Sci. **NS-27**, 1829–1833 (1980).
34. K. S. Kunz and L. Simpson, "A technique for increasing the resolution of finite-difference solution of Maxwell equation," IEEE Trans. Electromagn. Compat. **EMC-23**, 419–422 (1981).
35. C. T. Tai, *Dyadic Green's Functions in Electromagnetic Theory* (International Textbook, Scranton, Pa., 1971), Chap. 4, p. 48.
36. D. S. Saxon, "Lectures on the scattering of light," in Proceedings of the UCLA International Conference on Radiation and Remote Probing of the Atmosphere (West Periodicals, North Hollywood, Calif., 1973), pp. 227–308.
37. J. D. Jackson, *Classical Electrodynamics*, 2nd ed. (Wiley, New York, 1975).
38. M. Furse, S. P. Mathur, and O. P. Gandhi, "Improvements on the finite-difference time-domain method for calculating the radar cross section of a perfectly conducting target," IEEE Trans. Microwave Theory Tech. **38**, 919–927 (1990).
39. S. Asano and M. Sato, "Light scattering by randomly oriented spheroidal particles," Appl. Opt. **19**, 962–974 (1980).
40. Y. Takano and K. N. Liou, "Radiative transfer in cirrus clouds. Part III. Light scattering by irregular ice crystals," J. Atmos. Sci. **52**, 818–837 (1995).